Current Research in Food Science 10 (2025) 101049

Contents lists available at ScienceDirect

Current Research in Food Science

journal homepage: www.sciencedirect.com/journal/current-research-in-food-science

Investigating the interaction between tangeretin metabolism and amelioration of gut microbiota disorders using dextran sulfate sodium-induced colitis and antibiotic-associated diarrhea models

Jingyi Xu [a], Yilu Chen [b], Minmin Zhan [c], Shijun Liu [d], Huikun Zhang [a], Qianhua Wu [a], Jie Xiao [a], Yong Cao [a], Hang Xiao [b], Mingyue Song [a,*]

[a] Guangdong Provincial Key Laboratory of Nutraceuticals and Functional Foods, College of Food Sciences, South China Agricultural University, Guangzhou, China
[b] Department of Food Science, University of Massachusetts, Amherst, MA, 01003, USA
[c] Department of Food Science and Nutrition, College of Biosystems Engineering and Food Science, Zhejiang University, Hangzhou, China
[d] Guangzhou Institute of Energy Conversion, Guangzhou, China

ARTICLE INFO

Handling Editor: Dr. Quancai Sun

Keywords:
Tangeretin
Gut microbiota
Homeostasis
Fermentation in vitro
Metabolism

ABSTRACT

Dysregulation of gut microbiota homeostasis can lead to various health issues. In this study, we investigated the effects of tangeretin (TAN) on gut microbiota homeostasis in a mouse model (C57BL/6J) of disease, specifically focusing on dextran sulfate sodium (DSS)-induced colitis and antibiotic-associated diarrhea through in vitro fermentation of intestinal bacteria. Our results demonstrated that TAN effectively improved the diversity and structure of the disordered microbiota, increasing the levels of beneficial bacteria such as *Lachnospiraceae* and *Bacteroidaceae*, while decreasing harmful bacteria such as *Enterococcaceae* and *Pseudomonadaceae*. Additionally, TAN enhanced the production of short-chain fatty acids (SCFAs) in disordered microbial communities. Moreover, the metabolism of TAN by intestinal microorganisms yielded two new metabolites, which exhibited an inverse-conjugate (deconjugate) role, leading to the production of more functional substances with high bioactivity. These findings provide a scientific basis for the potential use of TAN as a prebiotic to regulate intestinal microbiota.

1. Introduction

The human gastrointestinal tract harbors a remarkably high density of microorganisms known as the microbiota, which consists of up to 100 trillion cells. This gut microbiota interacts with the host from birth, playing a crucial role in various functions such as immunity and metabolism. It facilitates the conversion of dietary nutrients into metabolites, which act as bioactive molecules to modulate host regulation. Additionally, probiotics within the gut microbiota can positively impact several major human diseases, often surpassing expectations (Xie and Liu, 2024; Chandrasekaran et al., 2024). Beyond its direct influence on human health, the gut microbiota also works synergistically with other body systems, including the microbiota-gut-liver axis. This axis, characterized by a bi-directional relationship between the gut and liver, regulates immunity, digestion, metabolism, and liver-related diseases, while promoting both physical and mental health (Bhardwaj and Mazumder, 2024). Therefore, maintaining a stable and healthy gut microbiota is crucial for optimal bodily function.

Dysregulation of gut microbiota homeostasis can be harmful not only to healthy individuals but also to those with existing diseases. One such condition, inflammatory bowel disease (IBD), results from a complex interplay of genetics, environment, microbiota, and immune-mediated factors. It is marked by reduced diversity in the intestinal flora and an overgrowth of harmful bacteria. This dysregulated microbiota overstimulates the gut's immune response, impairs the intestinal barrier, and exacerbates inflammation, potentially leading to chronic inflammation (Naito and Takagi, 2024). Similarly, antibiotic-associated diarrhea, a common complication of antibiotic therapy, arises when shifts in the composition and abundance of intestinal flora allow pathogenic overgrowth. This disruption can cause widespread metabolic disorders in the

* Corresponding author.
E-mail addresses: 276623420@qq.com (J. Xu), yiluchen@umass.edu (Y. Chen), 1069824054@qq.com (M. Zhan), liusj@ms.giec.ac.cn (S. Liu), 501391822@qq.com (H. Zhang), 15112142721@163.com (Q. Wu), xiaojieacademic@163.com (J. Xiao), caoyong2181@scau.edu.cn (Y. Cao), hangxiao@foodsci.umass.edu (H. Xiao), songmy@scau.edu.cn (M. Song).

https://doi.org/10.1016/j.crfs.2025.101049
Received 21 February 2025; Received in revised form 26 March 2025; Accepted 5 April 2025
Available online 7 April 2025

colon, mucosal dysfunction, and adverse outcomes like diarrhea (Wang et al., 2024a). The use of the gastrointestinally absorbed broad-spectrum antibiotics ampicillin and neomycin enables inhibition of the growth of both Gram-positive and Gram-negative bacteria, thereby facilitating the construction of an animal model of antibiotic-associated diarrhea (Xu et al., 2022; Rey et al., 2018). Additionally, intestinal dysbiosis can create a vicious cycle, leading to symptoms such as loss of appetite, vomiting, and diarrhea, which in turn compromise immune function and, in severe cases, negatively affect overall health. Thus, there is a need for effective preventive strategies to address microbiota imbalances and their detrimental effects on health.

TAN (4′,5,6,7,8-pentamethoxyflavone), one of the polymethoxyflavone (PMFs), abundantly found in citrus juices, seeds, peels, leaves, etc (Lv et al., 2023), has been shown to exhibit a wide range of biological activities, including anti-inflammatory, anti-obesity, anti-diabetic, and anti-cancer effects (Liu et al., 2023). These benefits are often linked to its metabolites, such as 5-demethyltangeretin and xanthomicrol (XAN), which have been reported to demonstrate stronger bioactive functions, particularly in anti-inflammatory roles (Guo et al., 2018). Previous research from our group has explored the mitigating effects of TAN on disease models, such as DSS-induced colitis and antibiotic-associated diarrhea, highlighting its positive impact on the gut microbiota, i.e., mitigating the effects of diseases on mice through structural adjustment, diversity restoration, and improvement in the ratio of beneficial to harmful bacteria in the intestinal flora, etc. The mechanism behind TAN's positive effects on the intestinal flora involves structural adjustment, restoration of diversity, and improving the balance between beneficial and harmful bacteria. This microbial modulation helps mitigate disease symptoms and restores the body to a healthy state, supporting the idea of TAN as an effective preventive health strategy (Chen et al., 2021, 2023). Moreover, similar to other compounds like curcumin, which undergoes metabolic conversion by the intestinal microbiota from the phase II metabolites (lower bioactivity) into the phase I metabolites (higher bioactivity and functionality), resulting in enhanced bioactivity (Luo et al., 2024), TAN may also experience metabolic transformation within the gut, potentially boosting its efficacy. In simpler terms, the beneficial effect of the gut microbiota on the body is twofold. First, the microbiota can improve the composition and balance of the gut flora by the action of functionally active substances, such as TAN. Second, the microbiota can metabolize external compounds, converting them into forms that have enhanced biological activity and better bioavailability. This metabolic conversion not only boosts the functional effectiveness of these substances but also ensures they can be more efficiently utilized by the body. Thus, the microbiota plays a key role in both maintaining a healthy gut ecosystem and enhancing the activity of beneficial compounds.

While previous studies have established the beneficial impact of TAN on gut flora, questions remain about whether these effects are directly substance-dependent or influenced by metabolic conversion. The complex body environment, including enzymes and bile acids, poses challenges in fully understanding the direct and indirect effects of TAN. To address these uncertainties, the current study aims to explore the relationship between TAN and gut microbiota by conducting in vitro fermentation experiments, thus excluding the potential interference of in vivo environmental factors. This investigation is crucial in validating whether TAN's modulation of the gut microbiota is solely attributable to the compound itself or enhanced through metabolic conversion, further elucidating its prebiotic effects. The findings could provide important insights into the mechanisms by which TAN exerts its beneficial effects, particularly in improving gut health and disease prevention.

2. Material and methods

2.1. Materials and reagents

The TAN (purity: 98 %) was supplied from Yuanzhi Biotechnology, Ltd. (Nanjing, China). DSS (molecular weight of 36,000–50,000 Da) was obtained from MP Biochemicals (Santa Ana, CA, U.S.A.). PMFs standards of potential TAN metabolites: gardenin B (GB) and hesperetin (HES) was purchased from Yuanye Bio-Technology Co., Ltd (Shanghai, China); XAN was purchased from BioBioPha (Yunnan, China). The ET fermentation medium was supplied by Hopebiol (Qingdao, China). Sulfatase from Helix pomatia was supplied from Sigma-Aldrich (St. Louis, MO). HPLC-grade methanol and acetonitrile were obtained from StarMark Science and Technology Development Co., Ltd (Tianjin, China).

2.2. Animal experiment design

The animal experiment was conducted in accordance with the regulations of the Animal Center of China and approved by the Animal Committee of South China Agricultural University (protocol number: 2023B172). Seventy male C57BL/6J mice were purchased from Charles River Laboratories (Beijing, China). The mice were housed under controlled conditions at 25 ± 2 °C and 65 % humidity, with a 12-h light/12-h dark cycle. During the first week, the mice were rotated between cages to normalize their initial gut microbiota, minimizing potential effects from maternal or cage-related factors. After a one-week acclimation period, the mice were divided into six groups as follows: the control group (CTL, n = 10) and the TAN group (TH, n = 10) received normal drinking water; the DSS-treated colitis group (DSS, n = 15) and the TAN + DSS group (TAN-D, n = 10) received 1.5 % DSS in drinking water (w/v); the antibiotic-treated diarrhea group (ANTI, n = 15) and the TAN + antibiotic-treated group (TAN-A, n = 10) received water containing 1.6 g/L ampicillin and 0.8 g/L neomycin sulfate. All groups were provided with a standard diet, and TAN was dissolved in medium chain triglycerides (MCT) solution for daily oral gavage. The TAN-D group received 180 ppm of TAN, while the TAN-A and TH groups were gavaged with 250 ppm of TAN. The CTL, DSS, and ANTI groups received an equivalent volume of MCT solution. The treatments were administered daily for 10 days, and all mice were sacrificed on the 17th day. The animal experiment design is shown in Fig. S1.

2.3. Preparation of fecal slurry

Fecal samples were collected from mice on the 16th day of the experiment and stored in a sterile anaerobic environment, following a modified protocol from a previous study (Liang et al., 2023). The fresh feces were mixed in equal proportions with sterile phosphate-buffered saline (PBS, 0.1 M, pH 7.0) to create a fecal slurry (10 %, w/v). The resulting fecal homogenate was then filtered through sterile gauze to obtain the fecal slurry for subsequent in vitro fermentation experiments.

2.4. Preparation of culture medium

The culture medium for in vitro fermentation of gut microbiota was prepared following a previously described method (Bai et al., 2023). The ET fermentation medium consisted of the following components (g/L): 2 g peptone, 2 g yeast extract, 0.1 g NaCl, 0.04 g potassium dihydrogen phosphate, 0.04 g dipotassium hydrogen phosphate, 0.01 g magnesium sulfate heptahydrate, 0.01 g calcium chloride hexahydrate, 2 g sodium bicarbonate, 0.5 g L-cysteine, and 0.5 g bile salt. To prepare the medium, 7.2 g of the mixed powder was combined with 35 mg of heme chloride, 2 mL of Tween 80, and 4 mL of resazurin solution (0.025 % w/v) in 1 L of distilled water. The mixture was then sterilized in a glass vessel at 121 °C for 20 min before fermentation.

2.5. Fermentation conditions

In vitro fermentation was performed following a previously described method with slight modifications (Chen et al., 2024). TAN was dissolved in a 0.5 % carboxymethylcellulose sodium (CMC-Na) solution,

filtered through a sterile filter, and placed in a sterile centrifuge tube. The final fermentation volume was 10 mL, consisting of 70 % culture medium, 20 % fecal slurry, and 10 % TAN solution (or a control without TAN). All samples were fermented under controlled anaerobic conditions (5 % CO_2 and 95 % N_2) at 37 °C. Following this, either the TAN solution or an equivalent volume of solvent was added for fermentation. Different fermentation broths were prepared by mixing solvents with or without TAN and various groups of fecal slurries (derived from the animal experiment in Section 2.2). Samples were collected for further analysis, and the fermentation was conducted in triplicate.

2.6. Plotting of growth curves

Fermentation samples were transferred to a 96-well cell culture plate. Absorbance at 600 nm was measured using a microplate reader (VersaMax, Molecular Devices, USA). Growth curves were plotted using GraphPad Prism software.

2.7. Measurement of SCFAs

SCFAs measurement was conducted using a method adapted from previous studies (Zhan et al., 2024). A 50 μL aliquot of fermentation sample was mixed with 200 μL of 0.5 % phosphoric acid solution (containing 4-methylpentanoic acid as an internal standard). An equal volume of ether was added, followed by centrifugation for 10 min at 4 °C and 14,000 rpm. The supernatants were analyzed by gas chromatography (GC, Agilent 7890B) equipped with a HP-INNOWax column.

2.8. Analysis of 16S rRNA

Total genomic DNA was extracted using a DNA Extraction Kit (Magan, Shanghai, China) following the manufacturer's instructions. DNA quality was assessed using a NanoDrop 2000 (Thermo Fisher Scientific, USA) and agarose gel electrophoresis. The extracted DNA served as a template for PCR amplification of bacterial 16S rRNA genes using barcoded primers and Takara Ex Taq (Takara, Japan). For bacterial diversity analysis, 16S rRNA genes were amplified with universal primers 343F (5′-TACGGRAGGCAGCAG-3′) and 798R (5′-AGGGTATCTAATCCT-3′). The quality of the amplicons was visualized using agarose gel electrophoresis, followed by purification and a second round of PCR amplification. The final amplicons were quantified using the Qubit dsDNA Assay Kit (Thermo Fisher Scientific, USA). The sequences were clustered into operational taxonomic units (OTUs) using Vsearch software with a 97 % pairwise identity threshold, and further analysis was conducted using QIIME software.

2.9. Metabolite extraction

The sample preparation procedure was adapted from a validated method with some modifications (Luo et al., 2024). The extraction solution was prepared by mixing acidified methanol and acetonitrile (0.1 % formic acid) in a 1:1 ratio (v/v). A total of 100 μL of fermentation samples was combined with 3200 μL of the extraction solution, and 0.0017 μM of HES was added as an IS. The mixture was vortexed and centrifuged for 15 min at 4 °C and 14,000 rpm. The supernatants were pooled and divided into two tubes for evaporation under vacuum (ZL2-1K, Ke Cheng, Hunan, China). One tube containing the solid was reconstituted in 200 μL of 50 % acetonitrile for subsequent LC/MS analysis. The second tube was used to measure the quantities of glucuronide, glycosylate, and sulfate metabolites through enzymatic hydrolysis. This tube was vortexed and sonicated with 90 μL of PBS (pH 5.0) and incubated with 10 μL of enzyme solution (100 mg/mL β-Glucuronidase from Helix pomatia, 100,000 units, pre-activated at 37 °C for 45 min) at 37 °C for 45 min. After incubation, the samples were mixed with 1600 μL of extraction solution, vortexed and sonicated, then centrifuged for 5 min at 4 °C and 14,000 rpm, and dried under vacuum. The resulting solid was reconstituted in 200 μL of 50 % acetonitrile for analysis.

2.10. LC-MS analysis

The LC-MS analysis was adapted from a validated method with some modifications (Luo et al., 2024). Mixed standards of TAN, GB, and XAN were prepared at concentrations of 0.008 μM, 0.017 μM, and 0.013 μM, respectively, resulting in Mixed Standard No. 8 (MSt 8). MSt 8 was subsequently diluted in ratios of 2.5, 5, 5, 2.5, 5, 5, and 5 to obtain Mixed Standards No. 7 through 1 (MSt 7–1). The mixed standards were extracted alongside the corresponding samples using the same sample preparation procedure.

UPLC-QTOF-MS/MS was used for the experiments. Specifically, an Agilent 6540 Q-TOF mass spectrometer equipped with a dual ESI source and interfaced it with an Agilent 1290 Infinity chromatographic system (Agilent Technologies, Santa Clara, CA, USA) were used. Chromatographic separation was accomplished by using an InfinityLab Poroshell 120 PFP column (4.6 × 150 mm, 2.7 μm particle size) (Agilent Technologies, Santa Clara, CA, USA). The operating parameters were as follows: positive ionization mode, gas temperature 350 °C, gas flow rate 10 L/min, nebulizer 55 psig, vcap 3500 V, skimmer 65 and fragmentor 175. MS2 results were acquired in TargetedMS2 mode over a mass range of 80–1200 m/z, with fixed collision energies set at 10/20/30/40 V. The mobile phase consisted of 0.05 % aqueous FA (A) and acetonitrile (B) containing 0.05 % FA. The flow rate was 0.6 mL/min. The linear gradient elution conditions were set as follows: 0–1 min, 5 % B; 1–3 min, 5–40 % B; 3–13 min, 40–65 % B; 13–19 min, 65–95 % B; 19–21 min, 95 % B; 21–23 min, 95-5 % B. The injection volume was 10 μL.

2.11. Statistical analysis

TAN metabolites were predicted using Metabolite software (Agilent Technologies, Santa Clara, CA, USA). Data analysis and processing were primarily performed with GraphPad Prism 9.5 (GraphPad Software, Inc., San Diego, CA, USA) and ChemDraw 20.0 (PerkinElmer, Inc., Waltham, MA, USA). Statistical significance was assessed using one-way parametric analysis of variance (ANOVA) followed by Tukey's post hoc test in GraphPad Prism 9.5. Results are presented as means ± standard error of the mean (SEM), with a p-value of less than 0.05 considered statistically significant.

3. Results and discussion

3.1. TAN improved the growth of DSS and antibiotic-induced disordered gut microbiota

Growth curves, commonly plotted in microbiology experiments by measuring OD600 (optical density at 600 nm), reflect the growth of microorganisms. These curves serve as an indicator of gut microbiota status, whether disordered or normal.

The intestinal microbiota was obtained by collecting fresh feces from mice, which had a flora status correlating with the mouse model. Gavage of TAN to different disease groups and normal mice successfully yielded the corresponding TAN-optimized flora. As shown in Fig. 1A and B, the gut microbiota of normal mice fed CMC-Na demonstrated a slight upward growth trend, indicating that the solvent was non-toxic and the culture environment was suitable. At 0 h, the values of disordered bacteria were similar, regardless of TAN administration, due to the colonies originating from the same model group. However, the abnormal flora resulting from DSS-induced disruption significantly differed from the normal flora at the same time point, consistent with findings that gut microbial diversity is associated with colonic inflammation (Haneishi et al., 2023). After TAN administration, the abnormal flora notably resumed growth, approaching the growth state of normal flora ($p < 0.05$). Notably, the optimized colonies from the TAN-D group

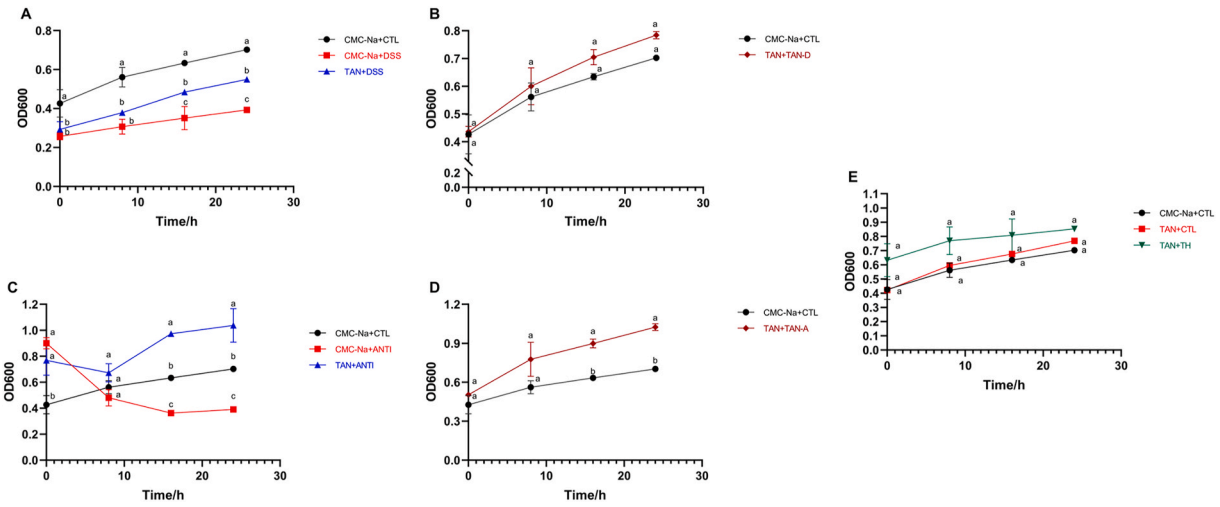

Fig. 1. Effect of TAN on gut microbiota growth. The absorbance values at 600 nm of the fermentation broths at 0, 8, 16 and 24 h were detected by a microplate reader and analyzed for comparison. (A) effect of TAN on abnormal microbiota induced by DSS treatment, (B) effect of TAN on optimized microbiota following DSS treatment, (C) effect of TAN on abnormal microbiota induced by antibiotic treatment, (D) effect of TAN on optimized microbiota following antibiotic treatment, (E) effect of TAN on normal and optimized microbiota. Different markers indicate the feeding substance (CMC-Na with or without TAN) and the source of gut microbiota (various sources of fecal slurry) (n = 3). Different letters (a, b, c) represent significant differences among groups at the same time point ($p < 0.05$, n = 3).

exhibited enhanced growth, aligning more closely with the normal growth trend.

As illustrated in Fig. 1C, the OD600 values of antibiotic-induced disordered flora were higher than those of normal flora at 0 h, regardless of TAN feeding, due to a darker fecal slurry color. There was a significant decrease in antibiotic-induced microbiota dysbiosis compared to normal flora, suggesting that the abnormal microbiota underwent autolysis ($p < 0.05$), negatively impacting intestinal

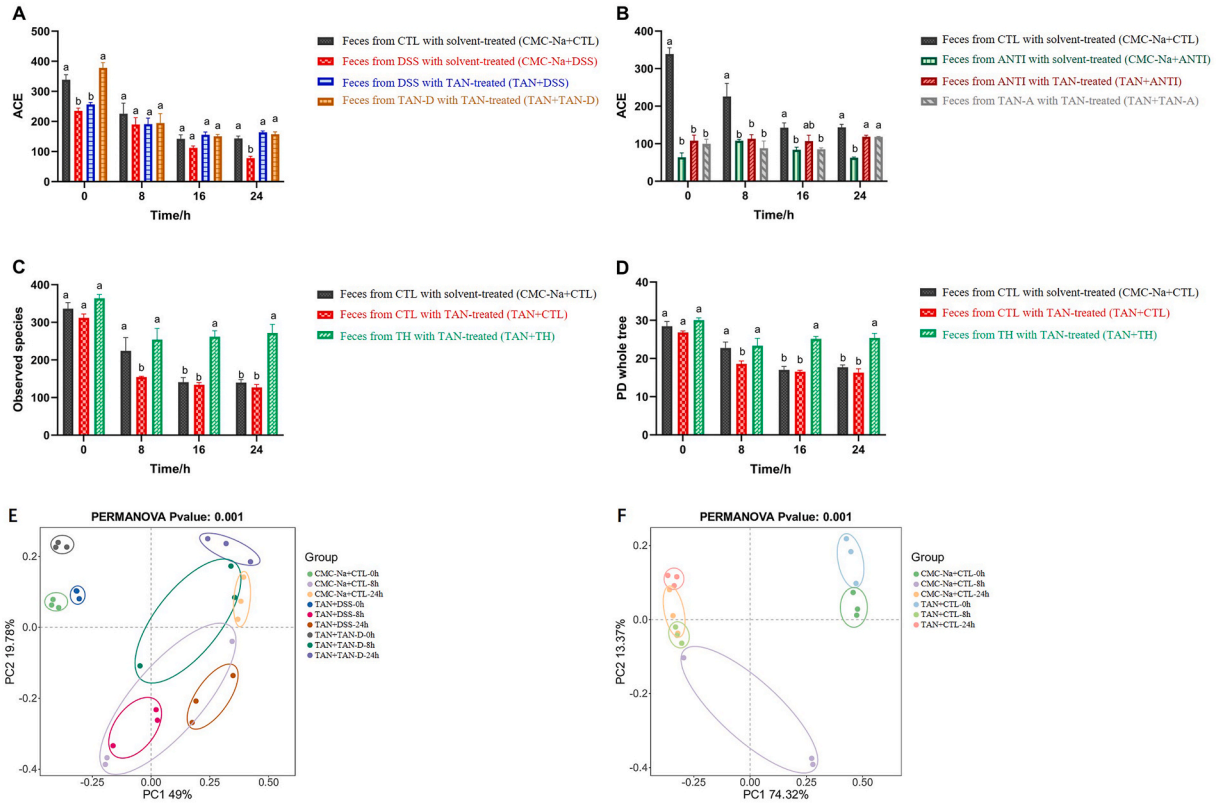

Fig. 2. Effect of TAN on the diversity of the gut microbiota. For disordered and TAN-optimized gut microbiota, α-diversity was assessed by ACE, observed species and the PD whole tree, while β-diversity was assessed by PCOA. α-diversity: (A) effect of TAN on abnormal and optimized microbiota induced by DSS treatment, assessed by ACE analysis, (B) effect of TAN on abnormal and optimized microbiota induced by antibiotic treatment, assessed by ACE analysis, (C) effect of TAN on normal and optimized microbiota, assessed by observed species analysis, (D) effect of TAN on of normal and optimized microbiota, assessed by PD whole tree analysis. β-diversity: (E) effect of TAN on abnormal and optimized microbiota induced by DSS treatment, (F) effect of TAN on normal microbiota. Different markers represent feeding substance (CMC-Na with or without TAN) + source of gut microbiota (different sources of fecal slurry). Different letters (a, b, c) represent significant differences for different groups at the same time ($p < 0.05$, n = 3).

function, metabolism, and the immune system (Yang et al., 2024). Although the disordered flora fed TAN showed a decreasing trend until 8 h, TAN significantly mitigated the decline of the microbial community after acclimatization, facilitating growth and reproduction that eventually surpassed that of the normal microbial community in later stages ($p < 0.05$). Moreover, the optimized microbiota from TAN-A-fed mice followed a similar growth pattern to the normal flora and was significantly better after 16 h (Fig. 1D, $p < 0.05$). Furthermore, as shown in Fig. 1E, the optimized flora of the TH group fed TAN exhibited a growth profile closely resembling that of the normal flora.

In conclusion, the gut maintains a stable microbiota that is crucial for overall health. TAN effectively alleviates growth decline caused by dysbiosis and gut microbiota disorders, even promoting recovery to a level comparable to that of healthy normal flora. Additionally, the optimized gut microbiota obtained from TAN demonstrates excellent growth activity.

3.2. TAN improved the diversity of the gut microbiota in DSS, antibiotic-treated, and normal mice

Previous studies have shown that patients with IBD exhibit altered gut microbial profiles compared to healthy individuals, leading to gut microbiota disorders (Pandey et al., 2024). Similarly, antibiotic-associated diarrhea is often linked to reduced gut microbial diversity and an altered abundance of certain taxa, a condition observed across various age groups (Abad and Safdar, 2021). These disruptions in the gut microbiota can further harm human health. Therefore, understanding how TAN positively impacts the gut microbiota is crucial. In this study, we first assessed the impact of TAN on the α-diversity of gut microbiota by evaluating ACE, observed species, and the PD whole tree. As shown in Fig. 2A, under anaerobic culture conditions, the diversity of normal microbiota decreased due to the death of aerobic bacteria. The DSS-induced disordered flora exhibited a significant reduction in diversity compared to normal flora ($p < 0.05$). However, after TAN administration, the diversity of the abnormal flora improved significantly ($p < 0.05$), with TAN-optimized bacteria achieving a diversity level comparable to that of healthy flora. In Fig. 2B, we show that TAN significantly mitigated the reduction in microbiota diversity caused by antibiotics, bringing it closer to the diversity observed in the normal microbiota ($p < 0.05$). Furthermore, for the optimized microbiota from the TH group, feeding TAN significantly increased the number of bacterial species and improved the overall PD tree, with this effect being time-dependent (Fig. 2C and D; $p < 0.05$).

Bacterial β-diversity, assessed through principal coordinate analysis (PCOA) of the Bray-Curtis index, revealed the relative similarity among different groups. As shown in Fig. 2E, the diversity of DSS-induced disordered and TAN-optimized microbiota approached that of normal colonies with increasing incubation time, with the TAN-optimized microbiota demonstrating a higher degree of similarity. The first two principal coordinates explained 68.78 % of the variance among the different groups. Moreover, the diversity of normal microbiota largely overlapped with that of the TAN-fed groups, further validating TAN's effect on microbial diversity (Fig. 2F), which accounted for 87.69 % of the variance.

In conclusion, TAN effectively improves the diversity of disease-induced disordered microbiota, bringing it closer to the profile of a healthy microbiota. This suggests that TAN can help mitigate disease-induced gut microbiota disruption by enhancing diversity.

3.3. TAN shifted the structure of the DSS, antibiotic-affected, and normal gut microbiota

Our previous studies have shown that diseases lead to imbalances in gut microbiota, negatively affecting its structure, and that improving dysbiosis can promote disease prevention (Chen et al., 2021, 2023). To better understand the impact of TAN on the gut microbiota, in this study, we identified the colonies by assessing the relative abundance of major taxa in each group. Fig. 3 visualizes the dominant microbiota among different gut colonies compared to normal colonies using linear discriminant analysis effect sizes (LEfSe). As illustrated in Fig. 3A and B, compared to normal microbiota, the DSS-induced disordered and TAN-optimized colonies exhibited an increase in the dominance of *Enterococcaceae*, *Lachnospiraceae* and *Erysipelatoclostridiaceae* over time. Conversely, as shown in Fig. 3C and D, *Bacteroidaceae* and *Tannerellaceae* became dominant in the antibiotic-induced disordered and TAN-optimized microbiota with increasing incubation time.

To assess changes in microbiota composition and relative abundance at the family and genus levels, we analyzed the gut microbiota of DSS-induced disordered and TAN-optimized microbiota, as shown in Fig. 4A. Major families identified included *Enterobacteriaceae*, *Enterococcaceae*, *Lachnospiraceae*, *Erysipelotrichaceae*, *Atopobiaceae*, *Bacteroidaceae* and *Peptostreptococcaceae*. Notably, the relative abundance of *Enterococcaceae* increased in the disordered colonies after DSS treatment, but TAN feeding significantly reduced its levels, gradually bringing them closer to those of the healthy colonies over time ($p < 0.05$). Previous studies have shown a significant increase in the relative abundance of *Enterococcaceae* in high-fat diet mice, suggesting that this pathogenic bacterium increased the risk of obesity (Liu et al., 2021). In contrast, the relative abundance of *Lachnospiraceae* decreased in the DSS-induced disordered colonies but increased in both the TAN-fed disordered and TAN-optimized colonies at 24 h ($p < 0.05$), which aligns with our previous in vivo mouse studies (Chen et al., 2021). *Lachnospiraceae* has been shown to increase butyric acid levels in SCFAs and reduce inflammation in gestational diabetes, thus resisting insulin resistance induced by high-fat diets (Huang et al., 2023). Importantly, the relative abundance of *Bacteroidaceae* in DSS-induced disordered colonies decreased dramatically over time, but TAN feeding restored and significantly increased its levels. Furthermore, the relative abundance of *Bacteroidaceae* in the TAN-optimized microbiota increased significantly when compared to the normal colonies ($p < 0.05$). Previous research has shown that *Bacteroidaceae* abundance is positively correlated with acetic acid levels and can play a beneficial role in modifying lipid metabolism (Yan et al., 2023).

As depicted in Fig. 4B, the gut microbiota of antibiotic-induced disordered and TAN-optimized colonies primarily consisted of *Bacteroidaceae*, *Tannerellaceae*, *Lachnospiraceae*, *Peptostreptococcaceae*, and *Pseudomonadaceae*. Interestingly, in the antibiotic-induced group, both disordered and TAN-optimized microbiota exhibited a significant increase in the proliferation of *Bacteroidaceae* compared to normal colonies. However, TAN feeding significantly mitigated this proliferation, reducing the relative abundance of *Bacteroidaceae* ($p < 0.05$). Previous studies have demonstrated that the use of neomycin in antibiotics resulted in an increase in the abundance of *Bacteroidaceae* (Yoon et al., 2022). It is important to note that TAN was not able to restore the levels of *Bacteroidaceae* to those seen in the normal flora, likely due to the high relative abundance of this bacterium at 0 h post-antibiotic exposure. Additionally, antibiotic treatment led to increased relative abundance of *Pseudomonadaceae*, which significantly differed from normal flora at 16 h. In contrast, TAN was able to significantly reduce its relative abundance ($p < 0.05$). Previous research has found an increased abundance of *Pseudomonadaceae* in the biliary microbiome of patients with biliary obstruction, which can affect both the liver and gut (Piyush and M, 2024).

After investigating the ability of TAN to alleviate disordered microbiota, we examined whether TAN could positively influence the normal flora and TAN-optimized microbiota, exploring its potential "prebiotic" effects. As shown in Fig. 4C, the normal and TAN-optimized microbiota at the family level were mainly composed of *Enterococcaceae*, *Lachnospiraceae*, *Atopobiaceae*, *Bacteroidaceae*, *[Eubacterium]_coprostanoligenes_group*, and *Lactobacillaceae*. Notably, the relative abundance of *Lachnospiraceae* significantly increased after TAN feeding in TAN-optimized colonies, a trend also observed in normal microbiota ($p <$

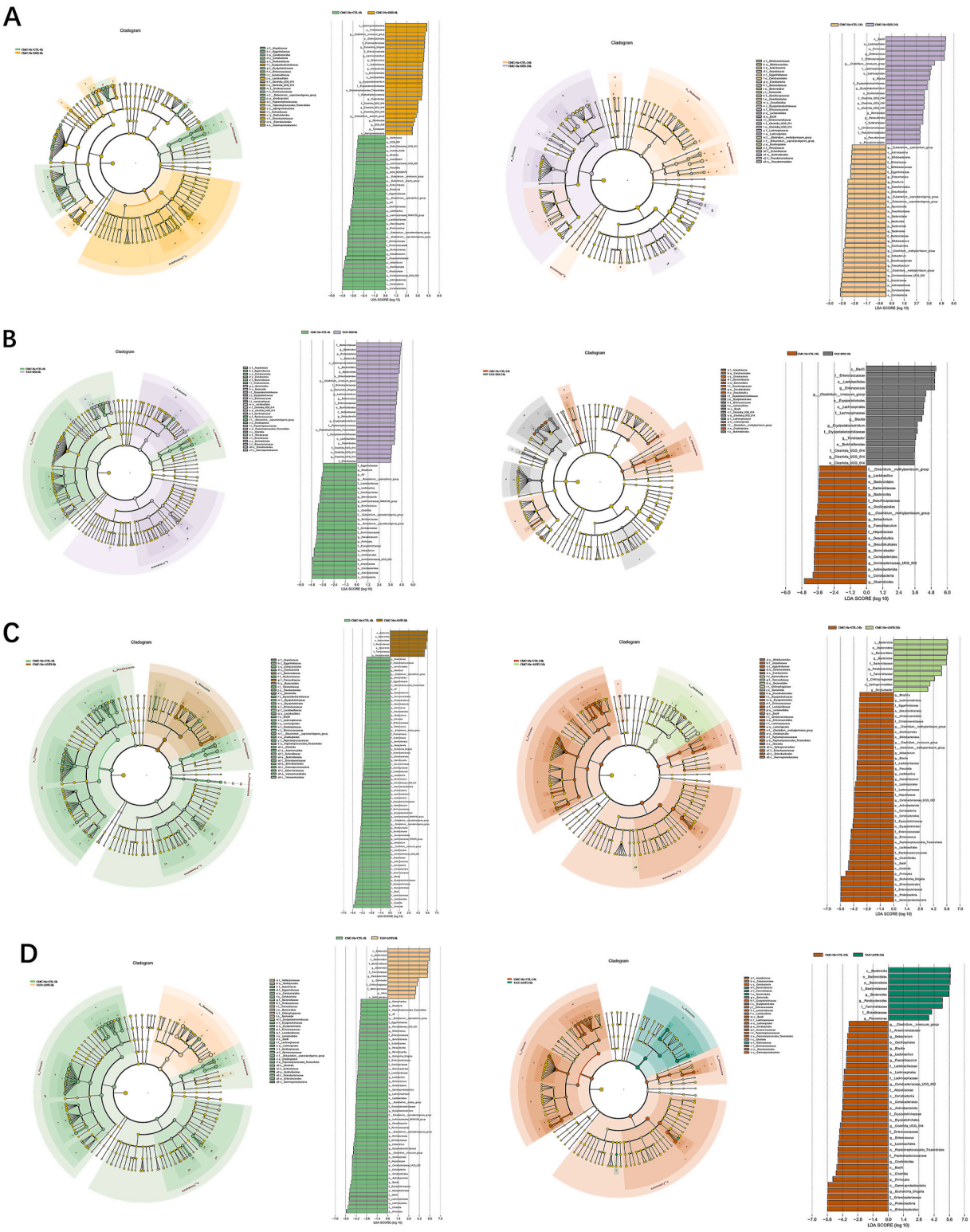

Fig. 3. LEfSe analysis of gut microbiota. Cladogram and LDA score analyses were used to determine the dominant microorganisms in the different models. Normal microbiota compared with (A) DSS-induced abnormal microbiota at 0 and 24 h, (B) DSS-induced abnormal microbiota with TAN fed at 0 and 24 h, (C) antibiotic-induced abnormal microbiota at 0 and 24 h, (D) antibiotic-induced abnormal microbiota with TAN fed at 0 and 24 h.

0.05). Additionally, the relative abundance of *Atopobiaceae* was significantly higher in both normal and TAN-optimized colonies after TAN feeding compared to normal colonies fed the solvent, with TAN-optimized colonies showing significantly higher levels than normal colonies at various time points ($p < 0.05$). *Atopobiaceae* has been associated with reduced inflammation and improved insulin resistance (Chang and Chen, 2021).

Next, we analyzed the relative abundance at the genus level. As shown in Fig. S2A, the DSS-induced disordered and TAN-optimized flora mainly consisted of Escherichia-*Shigella*, *Enterococcus*, *Coriobacteriaceae_UCG-002*, *Blautia*, *Clostridioides* and *Lactobacillus*. Notably, feeding TAN to disordered colonies effectively increased the relative

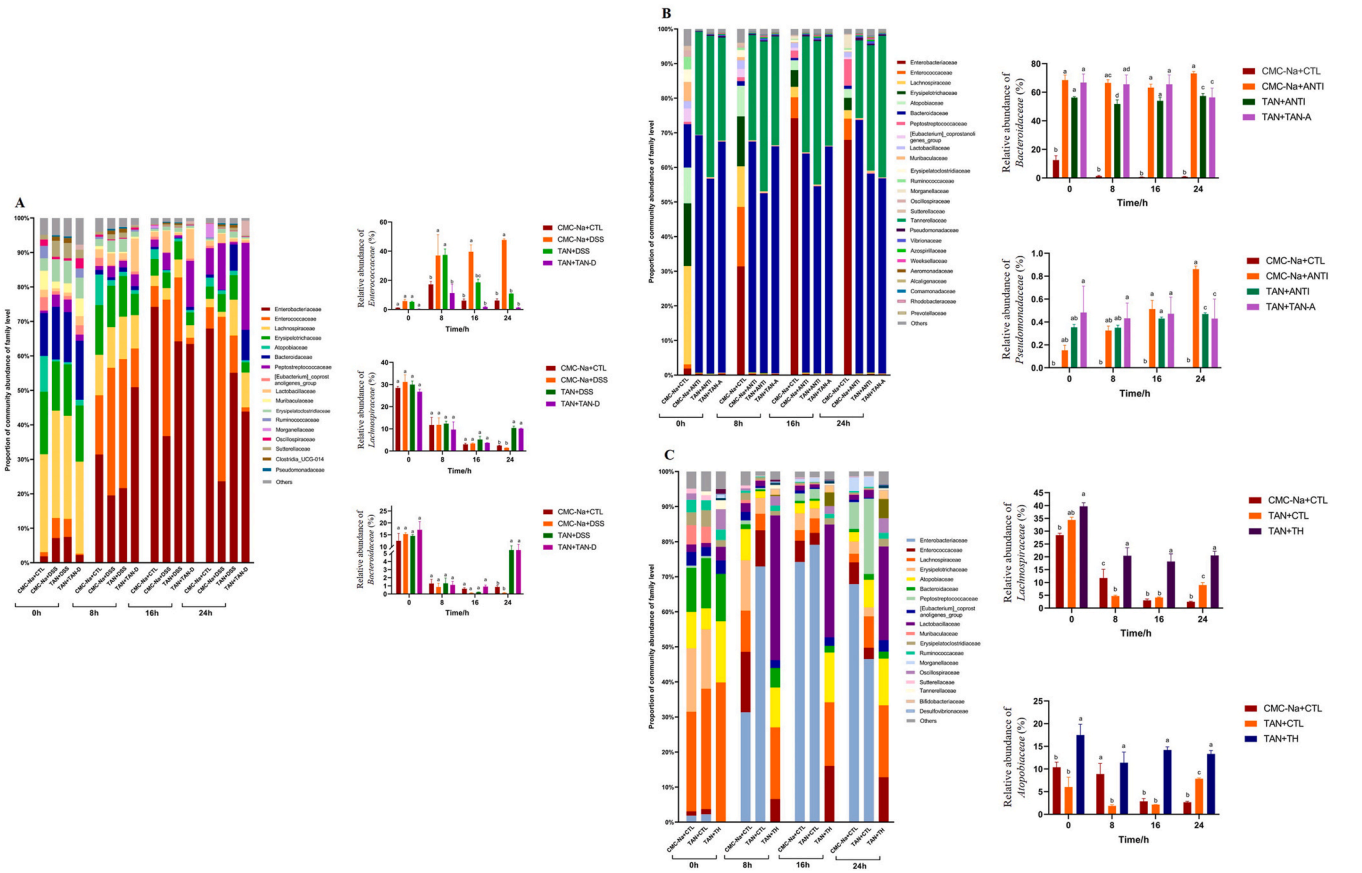

Fig. 4. Effect of TAN at the family level on the relative abundance of gut microbiota. For the abnormal and TAN-optimized microbiota, the relative abundance of beneficial and harmful bacteria was analyzed and compared with the normal microbiota. (A) Effect of TAN on the abnormal microbiota and TAN-optimized microbiota induced by DSS. (B) Effect of TAN on the abnormal microbiota and TAN-optimized microbiota induced by antibiotics. (C) Effect of TAN on the normal microbiota and TAN-optimized microbiota. Different markers represent the feeding substance (CMC-Na with or without TAN) and the source of the gut microbiota (different sources of fecal slurry). Different letters (a, b, c, d) indicate significant differences between groups at the same time point ($p < 0.05$, $n = 3$).

abundance of *Blautia*, compared to its reduced levels in the DSS-induced disordered microbiota. This trend was also observed in the TAN-optimized microbiota ($p < 0.05$). Previous studies have suggested that *Blautia* is involved in acetic acid production in lead-exposed mice on a high-fat diet and can help alleviate metabolic disorders in obese individuals exposed to heavy metals (Wang et al., 2024b). Conversely, the relative abundance of *Enterococcus* was significantly higher in DSS-induced disordered colonies, while TAN feeding significantly decreased its levels in both disordered and TAN-optimized colonies ($p < 0.05$). Increased *Enterococcus* abundance has been associated with ulcerative colitis, Crohn's disease, and ischemic colitis, indicating a strong link to intestinal inflammation (Dahal et al., 2023). Additionally, the relative abundance of *Erysipelatoclostridium* increased significantly in DSS-induced disordered microbiota, but TAN feeding reduced its levels by more than 50 %, moving closer to normal flora ($p < 0.05$). *Erysipelatoclostridium* has been associated with hyperuricemic nephropathy and positively correlates with uric acid levels, suggesting a link to nephropathy (Yu et al., 2024).

As illustrated in Fig. S2B, TAN-affected antibiotic-induced disordered and optimized microbiota consisted mainly of *Escherichia-Shigella*, *Bacteroides*, *Parabacteroides*, and *Pseudomonas*. Notably, the relative abundance of *Parabacteroides* in antibiotic-induced disordered microbiota was significantly higher than in normal flora, and TAN feeding effectively increased its levels ($p < 0.05$). Previous studies have shown that, despite *Parabacteroides*' resistance to antibiotics, it remains a beneficial bacterium capable of modulating immunity, relieving inflammation, and producing SCFAs (Zhou et al., 2024a; Yanlong et al., 2022). In addition, the relative abundance of *Vibrio*, which is associated with inflammation (Park et al., 2024), increased in the antibiotic-induced disordered microbiota, while feeding TAN significantly reduced its relative abundance ($p < 0.05$). Lastly, we observed a significant increase in the relative abundance of *Pseudomonas* in disordered flora, but TAN feeding resulted in a significant decrease ($p < 0.05$). *Pseudomonas* has been linked to lung abscesses and IBD (Matsushima et al., 2024; Hernandez-Boussard et al., 2016). However, it is important to note that the antibiotics used in human cases of antibiotic-associated diarrhea are somewhat distinct from those commonly used in animal models. Specifically, antibiotics such as ampicillin, neomycin, and lincomycin hydrochloride are frequently used in mice modeling (Lai et al., 2023; Liu et al., 2024), whereas humans are typically treated with antibiotics such as amoxicillin and cephalosporins (Basaranoglu et al., 2023; Ramirez et al., 2020). Therefore, future research using animal models should consider the choice of antibiotics used in clinical studies.

For both normal and TAN-optimized microbiota, the major components included *Enterococcus*, *Coriobacteriaceae_UCG-002*, *Blautia*, *Bacteroides*, and *Lactobacillus* (Fig. S2C). When comparing normal colonies with TAN-optimized colonies, we found that TAN feeding significantly increased the relative abundance of *Bacteroides* ($p < 0.05$). Previous studies have shown that *Bacteroides* can metabolize and produce volatile compounds, especially SCFAs, which positively affect intestinal immunity (Shagaleeva et al., 2023). Importantly, the relative abundance of *Blautia* increased significantly in both normal and TAN-optimized colonies after TAN feeding ($p < 0.05$). *Blautia* has been shown to reduce lipid accumulation, weight gain, and elevated blood glucose in type 2 diabetic mice, alleviating diabetic symptoms (Guo et al., 2024).

Additionally, the relative abundance of *Faecalibaculum* in normal and TAN-optimized colonies significantly increased after TAN feeding ($p < 0.05$). *Faecalibaculum* has been shown to produce SCFAs, which are associated with the alleviation of ulcerative colitis (Hu et al., 2023).

In summary, we conclude that TAN contributes to alleviating disease-induced gut microbiota disorders by modifying the microbiota structure, particularly by reducing harmful flora and increasing beneficial bacteria to promote overall health. While this process may take time, it can also have a positive effect on healthy microbiota, acting as a "prebiotic".

3.4. TAN restored SCFAs production in DSS- and antibiotic-affected gut microbiota

SCFAs, including acetic acid, isobutyric acid, butyric acid, and valeric acid, are end-products of the fermentation of indigestible dietary carbohydrates by commensal gut microorganisms. These SCFAs offer a range of health benefits, including anti-inflammatory, anti-tumor, and anti-obesity effects, and play a role in immune modulation for health promotion (Li et al., 2018, 2022). Butyric acid, in particular, helps maintain colon health by supporting the epithelial mucosa (Feng et al., 2018), while acetic acid is the most abundant SCFA in peripheral circulation and is involved in synthesizing glutamine and glutamate (Murugesan et al., 2018). Isobutyric acid, a branched-chain SCFA, which is proportional to the *Lactobacilli* level, has been shown to significantly enhance immune activity (Murayama et al., 2024; Zhao et al., 2023).

Alterations in gut microbiota can significantly affect SCFA levels, which are closely associated with DSS-induced colitis and antibiotic-mediated diarrhea. In our experiment, we observed changes in SCFA production starting at 16 h of fermentation, so the productions of SCFAs at 0, 16, 24 h were analyzed. Data in Fig. 5 shows that gut microbiota from the DSS group exhibited reductions in acetic acid and valeric acid levels by 34 % and 67 % after 16 h, and by 33 % and 54 % at 24 h, respectively, compared to normal microbiota. However, TAN treatment effectively restored SCFA production in the DSS-disordered microbiota, significantly increasing acetic acid and valeric acid to levels comparable to the normal microbiota ($p < 0.05$). These findings align with previous inter-team results (Chen et al., 2021). Additionally, the TAN-optimized microbiota, fed with TAN and incubated for 16 and 24 h, showed increases in acetic acid levels by 15 % and 34 %, and butyric acid levels by 200 % and 179 %, respectively, compared to the normal flora in the control group ($p < 0.05$). Importantly, TAN significantly enhanced valeric acid levels in the TAN-optimized microbiota, with increases of 135 % and 64 % after 16 and 24 h of fermentation ($p < 0.05$). Furthermore, TAN promoted a significant increase in isobutyric acid levels by 150 % and 139 % after 16 and 24 h, respectively ($p < 0.05$). Changes in SCFA levels are closely linked to intestinal flora composition. Our study demonstrated that TAN promotes the proliferation of *Lachnospiraceae*, *Bacteroidaceae*, and *Blautia*, which are associated with SCFA metabolism. Interestingly, in contrast to our team's findings on the effects of TAN on antibiotic-associated diarrhea in vivo (Chen et al., 2023), the antibiotic-induced disordered flora showed a significant reduction in acetic acid levels by 74 % at 16 h and 30 % at 24 h during in vitro fermentation. However, feeding TAN to this antibiotic-induced flora resulted in a significant reduction in acetic acid levels ($p < 0.05$), likely due to the down-regulation of elevated *Bacteroidaceae* abundance caused by antibiotics.

In summary, TAN regulates SCFA production by gut microbiota, and this effect is closely linked to alterations in microbial composition.

3.5. Identification of TAN metabolites from disordered and TAN-optimized gut microbiota due to DSS and antibiotic treatment

The homeostasis of the gut microbiota plays a crucial role in the metabolism of exogenous dietary substances. It not only influences the absorption and utilization of external compounds but also contributes to various beneficial physiological effects. Previous studies have shown that interactions between the gut microbiota and dietary compounds can impact the intestinal barrier and substance metabolism (Basnet et al., 2023). More importantly, the reciprocal relationship between gut microbiota and the metabolism of natural dietary substances is vital for maintaining the body's overall metabolism and improving immune function (Zhou et al., 2024b; Toledo et al., 2024). However, disruptions in the gut microbiota, often caused by disease or imbalance, can negatively affect metabolism, immune regulation, and the organism's overall health (de Oliveira et al., 2021). Therefore, it is vital to explore how gut microbiota influence the metabolism of TAN and their role in this process.

To further explore the impact of TAN on the gut microbiota and how the microbiota mediates the transformation of TAN, we identified the

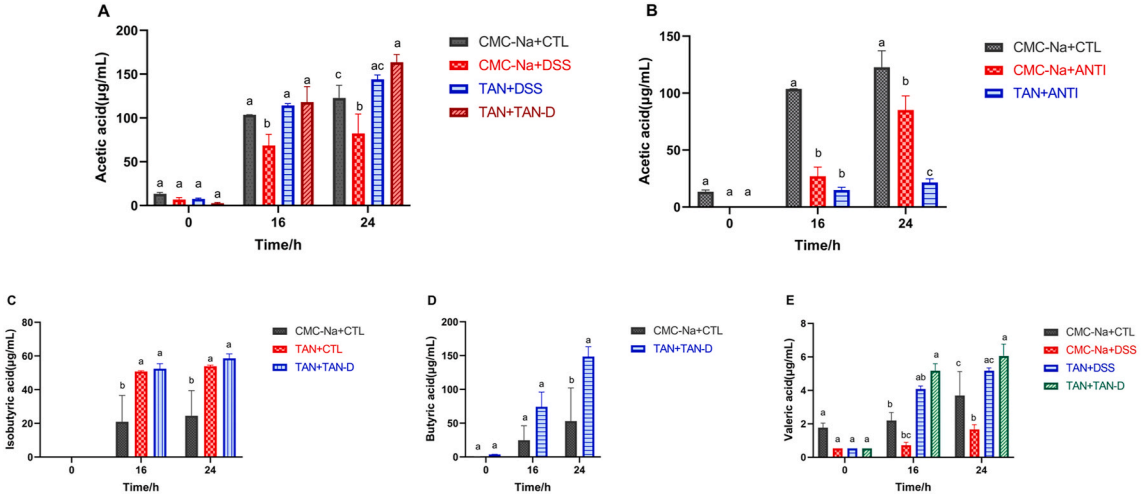

Fig. 5. TAN restored and promoted the production of SCFAs by gut microbiota. The levels of SCFAs at 0, 16, and 24 h were detected for the disordered and TAN-optimized microbiota by using GC and compared with those of the normal microbiota. (A) effect of TAN on acetic acid production by DSS-associated microbiota, (B) effect of TAN on acetic acid production by antibiotic-associated microbiota, (C) Effect of TAN on isobutyric acid production by DSS-treated TAN-optimized microbiota, (D) Effect of TAN on butyric acid production by DSS-treated TAN-optimized microbiota, (E) Effect of TAN on valeric acid production by DSS-treated TAN-optimized microbiota. Different markers represent the feeding substance (CMC-Na with or without TAN) and the source of gut microbiota (various fecal slurry sources). Distinct letters (a, b, c) indicate significant differences among groups at the same time point ($p < 0.05$, $n = 3$).

metabolites produced by the gut microbiota fed with TAN, using UPLC-QTOF-MS/MS in positive mode. The resulting metabolites varied under different experimental conditions, as detailed in Tables 1–3. These tables provide retention times (RTs), chemical formulas, and characteristic fragments. In these tables, 'M' represents compounds with the same formula, while differences in RTs and characteristic fragments indicate isomers (structural shifts of the compound).

RTs and fragmentation patterns of standards were used to identify TAN and its metabolites. As shown in Table 1, M0 at $[M+H]^+$ was m/z 373.1289, with error as 1.88 ppm, corresponding to $C_{20}H_{20}O_7$. The major fragments of M0 were observed at m/z 211.0228, 183.028, and 133.0621. In contrast, M1, M2, and M3 displayed protonated molecules at m/z 359.1113, 345.0979, and 343.1174, respectively, which align with previously reported values (Yu et al., 2022). Based on the RTs and fragmentation patterns, M1 and M2 were identified by comparing their data with corresponding standards. M1, with a RT of 14.137 min, was identified as GB, while M2, at 11.42 min, was identified as XAN. Other RTs for M1 and M2 represented functional group shifts of GB and XAN, respectively. Previous studies have shown that GB induces apoptosis and exhibits anticancer activity, while XAN inhibits cancer cell growth both in vitro and in vivo, and plays a significant role in the anti-inflammatory effects of M1 (Guo et al., 2018; Ghazizadeh et al., 2020; Cabrera et al., 2016). These data suggest that TAN, whether metabolized in vivo or fermented by gut microbiota in vitro, produces M1, M2, and M3. This supports the conclusion that these metabolites are among the most common and major metabolites of TAN.

The metabolite status of TAN in the abnormal and optimized gut microbiota, as influenced by ANTI treatment, is presented in Table 2. After confirmation through comparison with standards, M2 was identified as XAN with a RT of 11.413 min. However, contrary to previous studies, the metabolism of TAN by gut flora produced new metabolites that were distinct from those generated during in vivo metabolism. As predicted by ID and confirmed by MS2 analysis, M5 was identified as monodemethyl-demethoxy-tangeretin, which is 44 Da lighter than TAN (error: -9.12 ppm). The RDA fragment ions at m/z 119 were produced from the parent ion m/z 329 via the $[m/z\ 133\text{-}CH_2]^+$ and loss from the B ring, Similarly, m/z 211 resulted from $[M + H\text{-}2CH_3\text{-}CO]^+$ and loss from the A ring (Fig. 6A). We observed that both disordered and optimized microbiota in the antibiotic and TAN-A groups produced M1 and M3, while the optimized microbiota also generated M2 and M5, indicating that the TAN-optimized gut microbiota exhibited enhanced metabolic viability. Additionally, the different RTs of M5 in Table 1 are attributed to functional group displacement.

Table 3 presents metabolites from healthy and TAN-optimized microbiota, revealing a greater diversity than those from DSS- and antibiotic-treated microbiota. Analysis identified M4 as tridemethyl-tangeretin, with a protonated molecule at m/z 331.0809, consistent with previous reports (Yu et al., 2022). M6 was determined to be tetrademethyl-tangeretin, identified by the protonated molecule at m/z 317 (56 Da less than TAN, with a 7.88 ppm error), formed via $[m/z\ 133\text{-}CH_2]^+$ and the loss of the B-ring at RDA fragment m/z 119, and the loss of the A-ring at m/z 199 (Fig. 6B). Notably, both the healthy mice and those given TAN produced M1 and M3, while the TAN-optimized microbiota also produced M2, M4, M5, and M6. These additional metabolites may be linked to the enhanced growth and metabolic activity of the optimized microbiota.

In total, we identified six TAN metabolites (M0-M6), with M0 representing the parent compound (TAN). Future studies will further investigate the role of gut microbiota in influencing the metabolism of TAN.

3.6. Effect of DSS, antibiotic-affected, and normal gut microbiota on TAN metabolites

The state of gut microbiota significantly influences the metabolite profile of TAN. We quantified the metabolites and their conjugated forms (glucuronide, glycosylate, and sulfate metabolites) in response to DSS and antibiotic treatment, which disrupt gut flora and cause dysbiosis. Different fermentation broths were analyzed at 0, 8, 16, and 24 h to measure metabolite concentrations and their relative abundances.

As shown in Fig. 7A, the DSS-induced abnormal microbiota could still metabolize TAN to some extent. The free forms of M1 and M3 showed a slight increase, rising from 0.57 nmol/mL and 1 nmol/mL to 0.7 nmol/mL and 1.5 nmol/mL, respectively. However, the corresponding conjugated metabolites remained unchanged at their initial levels. Notably, M5 decreased from 0.13 nmol/mL to 0.11 nmol/mL, and its conjugated form was not detected, likely due to the absence of relevant bacteria. In contrast, Fig. 7B shows that the optimized microbiota from TAN gavage in DSS-induced mice not only metabolized more TAN but also exhibited varied content levels. For example, free forms of M1 and M2 increased from 50 nmol/mL and 83 nmol/mL to 61 nmol/mL and 117 nmol/mL, respectively, while M3 decreased from 1.4 nmol/mL to 1 nmol/mL. Although conjugated metabolites generally increased, the changes were modest.

Fig. 7C illustrates the effect of antibiotic-induced abnormal gut flora on TAN metabolism, revealing decreased levels of free metabolites (M1 and M3) and their conjugated forms. This reduction was likely due to the impaired metabolism resulting from the death of several microbiota species caused by antibiotic treatment. However, as shown in Fig. 7D, the optimized microbiota obtained by TAN gavage in antibiotic-treated mice exhibited an increase in certain free and conjugated metabolites. Specifically, M1 and M2 increased from 150 nmol/mL and 56 nmol/mL to 215 nmol/mL and 108 nmol/mL, respectively, while M3 decreased by half from 2.8 nmol/mL to 1.4 nmol/mL. Interestingly, M5 showed increased volatility, rising from 0 nmol/mL to 0.03 nmol/mL. More notably, M1-associated conjugates surged from 94 nmol/mL to 158 nmol/mL. On the other hand, as shown in Fig. 7E, the metabolites (both free and conjugated forms) from normal microbiota generally showed a decreasing or stable trend. However, the TAN-optimized flora obtained by TAN gavage in these mice (Fig. 7F) showed a decrease in free forms and an increase or stable trend in conjugated form metabolites. Regardless of DSS or antibiotic induction, significant changes in the metabolites were observed compared to the normal microbiota. These changes are hypothesized to result from disease induction leading to the death of specific gut microbiota, which possess different abilities to metabolize TAN, ultimately altering its metabolism.

The analysis of the same metabolites from abnormal and optimized microbiota across different models provides insights into the metabolic levels of different gut microbiota as they evolve over time. As shown in Fig. 8A, with the cultivation of DSS-induced disordered microbiota and

Table 1
Metabolites of TAN on the abnormal and TAN-optimized microbiota induced by DSS.

ID	RT (min)	Formula	Theoretical Mass (m/z) $[M+H]^+$	Experimental Mass (m/z) $[M+H]^+$	Error (ppm)	Characteristic Fragment ions
M0	11.586	$C_{20}H_{20}O_7$	373.1282	373.1289	1.88	211, 183, 133
M1	9.118 14.137	$C_{19}H_{18}O_7$	359.1125	359.1113	−3.34	227, 197, 169, 133
M2	7.539, 11.42	$C_{18}H_{16}O_7$	345.0969	345.0979	2.90	227, 197, 169, 119
M3	11.2342	$C_{19}H_{18}O_6$	343.1176	343.1174	−0.58	211, 181, 153, 133
M5	13.602	$C_{18}H_{16}O_6$	329.102	329.1011	−0.27	211, 181, 153, 119

Table 2
Metabolites of TAN on the abnormal and TAN-optimized microbiota induced by antibiotics.

ID	RT (min)	Formula	Theoretical Mass (m/z) $[M+H]^+$	Experimental Mass (m/z) $[M+H]^+$	Error (ppm)	Characteristic Fragment ions
M0	11.562	$C_{20}H_{20}O_7$	373.1282	373.1284	0.54	211, 183, 133
M1	9.119, 9.395, 9.536	$C_{19}H_{18}O_7$	359.1125	359.1121	−1.11	227, 197, 169, 133
M2	7.534, 11.413	$C_{18}H_{16}O_7$	345.0969	345.097	0.29	197, 169, 119
M3	11.218	$C_{19}H_{18}O_6$	343.1176	343.1153	−6.70	211, 181, 153, 133
M5	8.819	$C_{18}H_{16}O_6$	329.102	329.099	−9.12	211, 181, 153, 119

Table 3
Metabolites of TAN on the normal and TAN-optimized microbiota.

ID	RT (min)	Formula	Theoretical Mass (m/z) $[M+H]^+$	Experimental Mass (m/z) $[M+H]^+$	Error (ppm)	Characteristic Fragment ions
M0	11.589	$C_{20}H_{20}O_7$	373.1282	373.1284	0.27	211, 183, 133
M1	9.127, 9.395, 9.557	$C_{19}H_{18}O_7$	359.1125	359.1121	−1.11	227, 197, 169, 133
M2	7.594, 8.012	$C_{18}H_{16}O_7$	345.0969	345.0968	−0.29	213, 182, 154, 133
M3	11.228	$C_{19}H_{18}O_6$	343.1176	343.1182	1.75	211, 181, 153, 133
M4	6.702	$C_{17}H_{14}O_7$	331.0812	331.0809	−0.91	213, 119
M5	13.555	$C_{18}H_{16}O_6$	329.102	329.1017	−0.91	211, 119
M6	7.492	$C_{16}H_{12}O_7$	317.0656	317.0681	7.88	199, 119

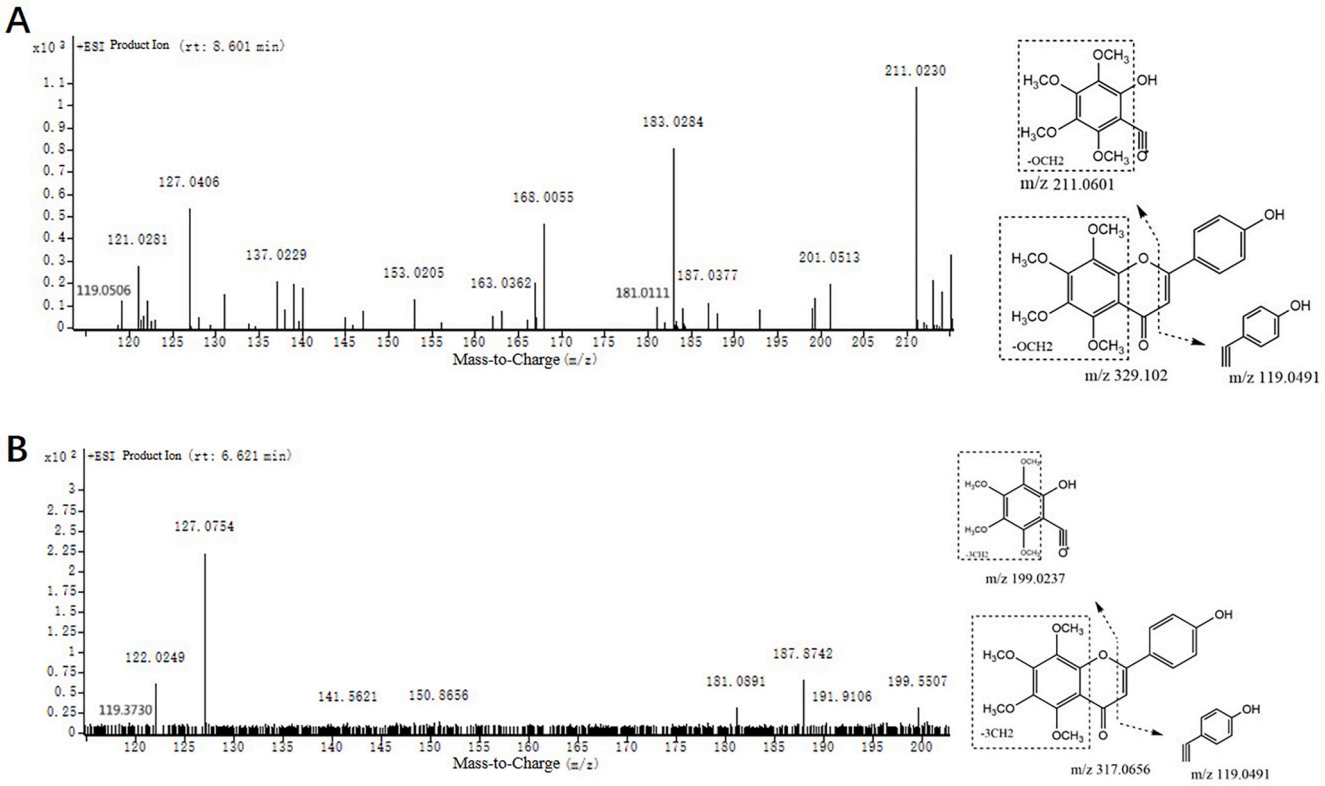

Fig. 6. Identification of TAN metabolites (MS2 spectrum). A total of six gut microbiota-associated TAN metabolites were identified by UPLC-QTOF-MS/MS, two of which were newly discovered. (A) M5 m/z 329, (B) M6 m/z 317.

TAN-optimized microbiota, both M1 and its conjugated forms increased. Notably, the metabolic level of the TAN-optimized microbiota significantly surpassed that of the disordered microbiota ($p < 0.05$). Similarly, in Fig. 8B, while the M1 content of the antibiotic-induced abnormal flora decreased, the M1 content in the TAN-optimized flora increased significantly ($p < 0.05$). In contrast, the content of M3 exhibited a decreasing trend in both the abnormal and TAN-optimized flora. Fig. 8C illustrates that changes in M1 and M3 contents in normal and TAN-optimized microbiota were relatively stable, with M3 gradually decreasing. Meanwhile, the M1-associated conjugates in the abnormal microbiota decreased, whereas those in the optimized microbiota increased. Combining Figs. 7 and 8, we observed non-unidirectional changes in some metabolite contents during the metabolic process. This is likely due to the absence or poor adaptation of specific microbiota. Some microbiota may have been absent at the early stages of metabolism, or the flora capable of producing certain metabolites may have struggled to

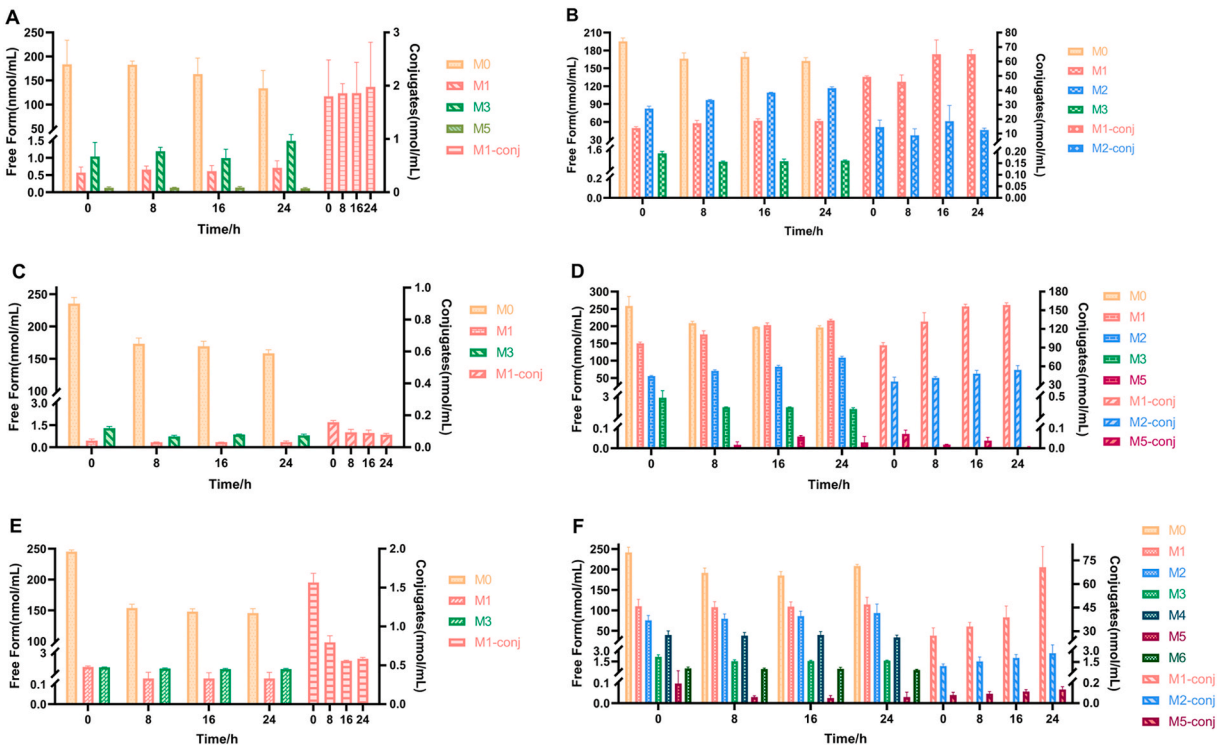

Fig. 7. Amounts of TAN metabolites and their conjugated forms produced by different gut microbiota. Quantitative analysis of free and conjugated metabolites of TAN by UP-LC-MS in positive mode. (A) microbiota from the DSS group, (B) microbiota from the TAN-D group, (C) microbiota from the ANTI group, (D) microbiota from the TAN-A group, (E) microbiota from the CTL group, (F) microbiota from the TH group (conj refers conjugates, n = 3).

grow, resulting in their eventual death. Alternatively, these changes might be attributed to the initial low relative abundance of certain bacteria caused by disease. However, as TAN was administered and the incubation period extended, these specific bacteria were able to proliferate and produce different metabolites.

We also summarized the proportions of free and conjugated metabolites in different gut microbiota. The free metabolites consisted of demethylated and demethoxylated forms of TAN, while the conjugated forms were the glucuronide, glycosylate, and sulfate metabolites derived from these free metabolites. Previous studies have shown that the intestinal flora has a strong ability to deconjugate metabolites of curcumin (Luo et al., 2024). Building on this premise, we further explored the role of gut flora in TAN metabolism. As shown in Fig. 9A and B, both DSS-induced and antibiotic-induced abnormal microbiota exhibited weak metabolic capacity, metabolizing only a small amount of metabolites. Coincidentally, at 0 h, the proportion of their TAN free-form metabolites was 50 % in both cases. Consequently, the ratio of free to conjugated forms remained largely unchanged after 8 h of incubation. This suggests that although the abnormal gut microbiota was somewhat alleviated by TAN, they remained in a dysfunctional state due to disease-induced dysregulation, which impaired their metabolic capacity. For the antibiotic-induced TAN-optimized microbiota, we observed a gradual decrease in the production of free metabolites and an increase in the production of conjugated metabolites. This trend was even more pronounced in the DSS-induced TAN-optimized microbiota. Specifically, at 24 h, the proportions of TAN free-form metabolites produced by DSS-induced disordered and TAN-optimized flora were 53.85 % and 69.87 %, respectively; whereas antibiotic-induced abnormal and TAN-optimized microbiota were 50 % and 60.63 %, respectively. Fig. 9C further illustrates that both normal and optimized microbiota exhibited a trend of increasing free forms and decreasing conjugated forms in TAN metabolism. Notably, the proportion of conjugated metabolites in normal microbiota decreased from 42 % to 33 % over 24 h. Overall, these findings suggest that the gut microbiota plays a deconjugating role in the metabolism of TAN, though this effect was not highly significant within the 24-h incubation period. This indicates that changes in the metabolic capacity of the microbiota require more time to become apparent than what was observed in this experiment.

As a result, we demonstrated that gut microbiota possess a strong ability to metabolize TAN through deconjugation, and this capability is enhanced with an increase in TAN-optimized flora.

4. Conclusion

In conclusion, we demonstrated the beneficial effects of TAN on gut microbiota disorders induced by disease, as exemplified by DSS-induced colitis and antibiotic-associated diarrhea. Specifically, TAN improved disordered flora by promoting diversity and enhancing structure—this included increasing the abundance of beneficial bacteria, reducing harmful bacteria, alleviating abnormal changes, and restoring SCFAs levels. TAN effectively reduced the proportion of harmful bacteria, thereby creating a more favorable environment for the growth and proliferation of beneficial bacteria. Specifically, TAN reduced the relative abundance of pathogenic bacteria, such as *Enterococcus* spp., and increased the relative abundance of beneficial bacteria. This shift promoted the production of short-chain fatty acids (SCFAs), which play a crucial role in maintaining intestinal health, modulating the immune system, and supporting intestinal barrier function. For instance, TAN increased the relative abundance of *Lachnospiraceae*, which ferments dietary fibers to produce acetic acid and butyric acid. These SCFAs provide energy to intestinal mucosal cells, reduce the production of pro-inflammatory cytokines, and support the integrity of the intestinal barrier. Additionally, TAN positively impacted normal intestinal flora, functioning as a “prebiotic”. We also identified two new metabolites of TAN under different gut microbiota conditions and confirmed the influence of altered flora on TAN metabolism by analyzing the relative contents of metabolites and their conjugates. Through metabolic processes, the gut microbiota is capable of converting conjugated

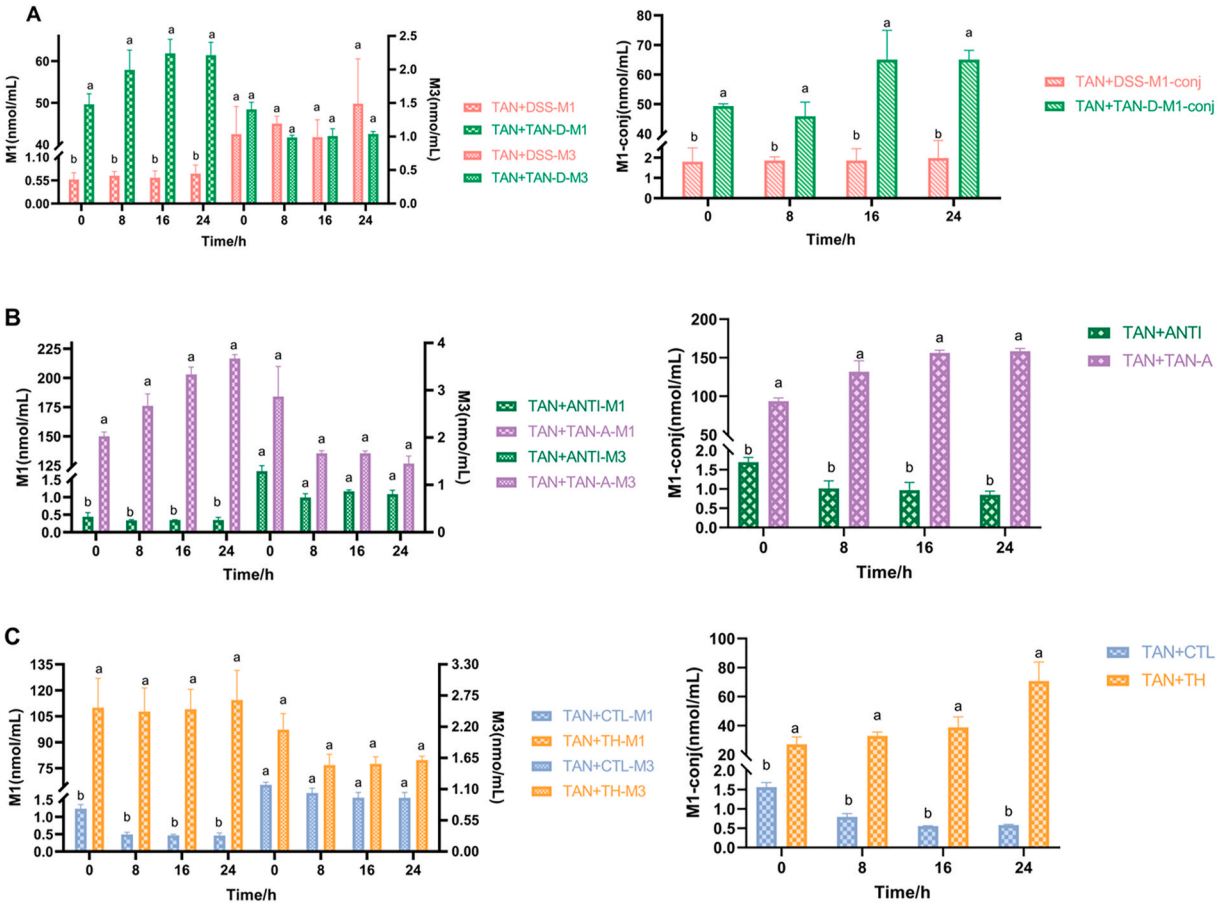

Fig. 8. Amounts of M1, M3 and their conjugated forms produced by different gut microbiota. Detection of M1, M3 and their conjugated form metabolites in different gut microbiota via UP-LC-MS in positive mode. (A) metabolic levels of TAN-optimized and abnormal microbiota from DSS-treated samples, (B) metabolic levels of TAN-optimized and abnormal microbiota from antibiotic-treated samples, (C) metabolic levels of TAN-optimized and normal microbiota from TAN-treated samples. Different markers represent the feeding substance (CMC-Na with or without TAN) and the source of the gut microbiota (different fecal slurry sources). Different letters (a, b) indicate significant differences between groups at the same time point ($p < 0.05$, $n = 3$).

metabolites, which have low or no functional activity, into free-form metabolites that possess greater bioactivity than TAN itself. For example, the metabolite GB (M1) of TAN demonstrated superior bioactivity compared to the parent compound (Charoensinphon et al., 2013), and the gut microbiota also plays a key role in the enhanced production of M1, increasing the bioactivity of TAN. Furthermore, both the normal and TAN-optimized microbiota exhibited improved inverse conjugation capacity. These findings suggest a direct and significant relationship between TAN-induced improvements in gut microbiota composition and the metabolic transformation that enhances TAN bioactivity. Overall, our findings suggest that TAN has a positive influence on disease-induced disruptions of the gut microbiota and holds potential as a health preventive strategy.

CRediT authorship contribution statement

Jingyi Xu: Data curation, Formal analysis, Investigation, Writing – original draft. **Yilu Chen:** Methodology. **Minmin Zhan:** Investigation, Visualization. **Shijun Liu:** Software. **Huikun Zhang:** Investigation, Resources, and. **Qianhua Wu:** Investigation, Resources. **Jie Xiao:** Validation, Supervision, Funding acquisition. **Yong Cao:** Validation, Supervision, Funding acquisition, and. **Hang Xiao:** Validation, Supervision, Funding acquisition. **Mingyue Song:** Conceptualization, Supervision, Writing – review & editing, Project administration, Funding acquisition.

Ethics statement

All animal procedures were performed in accordance with the Guidelines for Care and Use of Laboratory Animals of the "Regulations of Guangdong Province on the Management of Laboratory Animals" and approved by the Animal Ethics Committee of South China Agricultural University (Guangzhou, China, approval no. 2023B172).

Funding sources

This work was financially supported by the Program for Guangdong Introducing Innovative and Entrepreneurial Teams (2019ZT08N291), National Natural Science Foundation of China (32472353), Guangdong Provincial Natural Science Foundation (2025A1515011756) and the Guangdong Provincial Key Laboratory of Nutraceuticals and Functional Foods (2018B030322010).

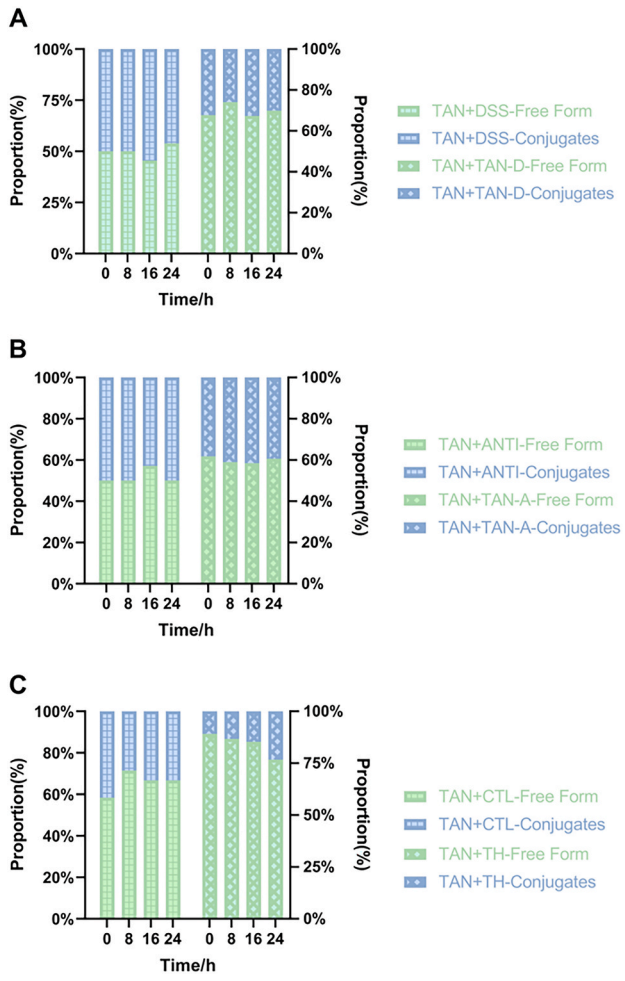

Fig. 9. Proportion of free and conjugated metabolites produced by different gut microbiota. (A) Proportion of metabolites from TAN-optimized and abnormal microbiota in DSS-treated samples. (B) Proportion of metabolites from TAN-optimized and abnormal microbiota in antibiotic-treated samples. (C) Proportion of metabolites from TAN-optimized and normal microbiota. Different markers represent the feeding substance (CMC-Na with or without TAN) and the source of the gut microbiota (different fecal slurry sources, n = 3).

Declaration of competing interest

There are no conflicts to declare.

Appendix A. Supplementary data

Supplementary data to this article can be found online at https://doi.org/10.1016/j.crfs.2025.101049.

Data availability

Data will be made available on request.

References

Abad, C.L.R., Safdar, N., 2021. A review of Clostridioides difficile infection and antibiotic-associated diarrhea. Clin. Gastroenterol. 50 (2), 323–340. https://doi.org/10.1016/j.gtc.2021.02.010.

Bai, Y., Zhou, Y., Li, X., et al., 2023. Longan pulp polysaccharides regulate gut microbiota and metabolites to protect intestinal epithelial barrier. Food Chem. 422, 136225. https://doi.org/10.1016/j.foodchem.2023.136225.

Basaranoglu, S.T., Karaaslan, A., Sali, E., et al., 2023. Antibiotic associated diarrhea in outpatient pediatric antibiotic therapy. BMC Pediatr. 23 (1), 121. https://doi.org/10.1186/s12887-023-03939-w.

Basnet, T.B., Gc, S., Basnet, R., et al., 2023. Interaction between gut microbiota metabolites and dietary components in lipid metabolism and metabolic diseases. Access Microbiol. 5 (6), i403. https://doi.org/10.1099/acmi.0.000403.

Bhardwaj, M., Mazumder, P.M., 2024. The gut - liver axis : emerging mechanisms and therapeutic approaches for nonalcoholic fatty liver disease and type 2 diabetes mellitus. N-S ARCH PHARMACOL 397 (11), 8421–8443. https://doi.org/10.1007/s00210-024-03204-6.

Cabrera, J., Saavedra, E., Rosario, H.D., et al., 2016. Gardenin B-induced cell death in human leukemia cells involves multiple caspases but is independent of the generation of reactive oxygen species. Chem. Biol. Interact. 256, 220–227. https://doi.org/10.1016/j.cbi.2016.07.016.

Chandrasekaran, P., Weiskirchen, S., Weiskirchen, R., 2024. Effects of probiotics on gut microbiota : an overview. Int. J. Mol. Sci. 25 (11), 6022. https://doi.org/10.3390/ijms25116022.

Chang, T., Chen, J., 2021. Direct CCL4 inhibition modulates gut microbiota , reduces circulating trimethylamine N-Oxide , and improves glucose and lipid metabolism in high-fat-diet-induced diabetes mellitus. J. Inflamm. Res. 14, 6237–6250. https://doi.org/10.2147/JIR.S343491.

Charoensinphon, N., Qiu, P., Dong, P., et al., 2013. 5-Demethyltangeretin inhibits human nonsmall cell lung cancer cell growth by inducing G2/M cell cycle arrest and apoptosis. Mol. Nutr. Food Res. 57 (12), 2103–2111. https://doi.org/10.1002/mnfr.201300136.

Chen, B., Luo, J., Han, Y., et al., 2021. Dietary tangeretin alleviated dextran sulfate sodium-induced colitis in mice via inhibiting inflammatory response, restoring intestinal barrier function, and modulating gut microbiota. J. Agric. Food Chem. 69 (27), 7663–7674. https://doi.org/10.1021/acs.jafc.1c03046.

Chen, B., Yang, X., Zhan, M., et al., 2023. Dietary tangeretin improved antibiotic-associated diarrhea in mice by enhancing the intestinal barrier function, regulating the gut microbiota, and metabolic homeostasis. Food Funct. 14 (24), 10731–10746. https://doi.org/10.1039/d3fo02998k.

Chen, X., Liu, S., Song, H., et al., 2024. Evaluation of biological activity and prebiotic properties of proanthocyanidins with different degrees of polymerization through simulated digestion and in vitro fermentation by human fecal microbiota. Food Chem. 447, 139015. https://doi.org/10.1016/j.foodchem.2024.139015.

Dahal, R.H., Kim, S., Kim, Y.K., et al., 2023. Insight into gut dysbiosis of patients with inflammatory bowel disease and ischemic colitis. Front. Microbiol. 14, 1174832. https://doi.org/10.3389/fmicb.2023.1174832.

de Oliveira, G.L.V., de Barros Cardoso, C.R., Taneja, V., et al., 2021. Editorial : intestinal dysbiosis in inflammatory diseases. Front. Immunol. 12, 727485. https://doi.org/10.3389/fimmu.2021.727485.

Feng, W., Ao, H., Peng, C., 2018. Gut microbiota , short-chain fatty acids , and herbal medicines. Front. Pharmacol. 9, 1354. https://doi.org/10.3389/fphar.2018.01354.

Ghazizadeh, F., Shafiei, M., Falak, R., et al., 2020. Xanthomicrol exerts antiangiogenic and antitumor effects in a mouse melanoma (B16F10) allograft model. Evidence-Based Complementary Altern. Med. 2020, 8543872. https://doi.org/10.1155/2020/8543872.

Guo, S., Wu, X., Zheng, J., et al., 2018. Anti-inflammatory effect of xanthomicrol, a major colonic metabolite of 5-demethyltangeretin. Food Funct. 9 (6), 3104–3113. https://doi.org/10.1039/C8FO00279G.

Guo, Q., Gao, Z., Zhao, L., et al., 2024. Multiomics analyses with stool - type stratification in patient cohorts and Blautia identification as a potential bacterial modulator in type 2 diabetes mellitus. Diabetes 73 (3), 511–527. https://doi.org/10.2337/db23-0447.

Haneishi, Y., Furuya, Y., Hasegawa, M., et al., 2023. Inflammatory bowel diseases and gut microbiota. Int. J. Mol. Sci. 24 (4), 3817. https://doi.org/10.3390/ijms24043817.

Hernandez-Boussard, T.M., Mcdonald, K.M., Morrison, D.E., et al., 2016. Risks of adverse events in colorectal patients : population-based study. J. Surg. Res. 202 (2), 328–334. https://doi.org/10.1016/j.jss.2016.01.013.

Hu, S., Ma, Y., Xiong, K., et al., 2023. Ameliorating effects of vitamin K2 on dextran sulfate sodium-induced ulcerative colitis in mice. Int. J. Mol. Sci. 24 (3), 2986. https://doi.org/10.3390/ijms24032986.

Huang, S., Chen, J., Cui, Z., et al., 2023. Lachnospiraceae - derived butyrate mediates protection of high fermentable fiber against placental inflammation in gestational diabetes mellitus. Sci. Adv. 9 (44), i7337. https://doi.org/10.1126/sciadv.adi7337.

Lai, Y., Deng, H., Fang, Q., et al., 2023. Water-insoluble polysaccharide extracted from poria cocos alleviates antibiotic-associated diarrhea based on regulating the gut microbiota in mice. Foods 12 (16), 3080. https://doi.org/10.3390/foods12163080.

Li, M., van Esch, B.C.A.M., Wagenaar, G.T.M., et al., 2018. Pro - and anti-inflammatory effects of short chain fatty acids on immune and endothelial cells. Eur. J. Pharmacol. 831, 52–59. https://doi.org/10.1016/j.ejphar.2018.05.003.

Li, C., Liang, Y., Qiao, Y., 2022. Messengers from the gut : gut microbiota-derived metabolites on host regulation. Front. Microbiol. 13, 863407. https://doi.org/10.3389/fmicb.2022.863407.

Liang, X., Liu, H., Wei, Z., et al., 2023. Modulation of gut flore by dietary fibers from Pyrus bretschneideri Rehd .: evaluation of fermentation characteristics using a colonic in vitro fermentation model. J. Funct.Foods 102, 105466. https://doi.org/10.1016/j.jff.2023.105466.

Liu, H., Zhu, H., Xia, H., et al., 2021. Different effects of high-fat diets rich in different oils on lipids metabolism , oxidative stress and gut microbiota. Food Res. Int. 141, 110078. https://doi.org/10.1016/j.foodres.2020.110078.

Liu, D., Liu, Y., Qian, X., et al., 2023. Pharmacokinetic study on the effect of ligustrazine - tangeretin co-administration on the pharmacokinetics of ligustrazine and its potential mechanism in rats. Pharmacol. Res. Perspect. 11 (2), e1058. https://doi.org/10.1002/prp2.1058.

Liu, S., Zhao, S., Cheng, Z., et al., 2024. Akkermansia muciniphila protects against antibiotic-associated diarrhea in mice. Probiotics Antimicrob. Proteins. 16 (4), 1190–1204. https://doi.org/10.1007/s12602-023-10101-6.

Luo, M., Han, Y., Chen, Y., et al., 2024. Unveiling the role of gut microbiota in curcumin metabolism using antibiotic-treated mice. Food Chem. 460, 140706. https://doi.org/10.1016/j.foodchem.2024.140706.

Lv, C., Li, Y., Liang, R., et al., 2023. Characterization of tangeretin as an activator of nuclear factor erythroid 2 - related factor 2/antioxidant response element pathway in HEK293T cells. Curr. Res. Food Sci. 6, 100459. https://doi.org/10.1016/j.crfs.2023.100459.

Matsushima, A., Mizuno, S., Minamikawa, S., et al., 2024. Pneumococcal pneumonia complicated by Aspergillus fumigatus and Pseudomonas aeruginosa lung abscesses. Pediatr. Pulmonol. 59 (4), 1077–1080. https://doi.org/10.1002/ppul.26854.

Murayama, M., Hosonuma, M., Kuramasu, A., et al., 2024. Isobutyric acid enhances the anti-tumour effect of anti-PD-1 antibody. Sci. Rep. 14 (1), 11325. https://doi.org/10.1038/s41598-024-59677-1.

Murugesan, S., Nirmalkar, K., Hoyo-Vadillo, C., et al., 2018. Gut microbiome production of short-chain fatty acids and obesity in children. Eur. J. Clin. Microbiol. Infect. Dis. 37 (4), 621–625. https://doi.org/10.1007/s10096-017-3143-0.

Naito, Y., Takagi, T., 2024. Role of gut microbiota in inflammatory bowel disease pathogenesis. J. Clin. Biochem. Nutr. 75 (3), 175–177. https://doi.org/10.3164/jcbn.24-112.

Pandey, H., Jain, D., Tang, D.W.T., et al., 2024. Gut microbiota in pathophysiology, diagnosis, and therapeutics of inflammatory bowel disease. Int. Res. 22 (1), 15–43. https://doi.org/10.5217/ir.2023.00080.

Park, J.E., Yun, J., Lee, W., et al., 2024. C-ter100 peptide derived from Vibrio vEP-45 protease acts as a pathogen-associated molecular pattern to induce inflammation and innate immunity. PLoS Pathog. 20 (8), e1012474. https://doi.org/10.1371/journal.ppat.1012474.

Piyush, B., M, M.S., 2024. The interplay of gut-microbiome between infection and inflammation. Front. Cell. Infect. Microbiol. 14, 1413473. https://doi.org/10.3389/fcimb.2024.1413473.

Ramirez, J., Guarner, F., Fernandez, L.B., et al., 2020. Antibiotics as major disruptors of gut microbiota. Front. Cell. Infect. Microbiol. 10, 572912. https://doi.org/10.3389/fcimb.2020.572912.

Rey, K., Manku, S., Enns, W., et al., 2018. Disruption of the gut microbiota with antibiotics exacerbates acute vascular rejection. Transplant 102 (7), 1085–1095. https://doi.org/10.1097/TP.0000000000002169.

Shagaleeva, O.Y., Kashatnikova, D.A., Kardonsky, D.A., et al., 2023. Investigating volatile compounds in the Bacteroides secretome. Front. Microbiol. 14, 1164877. https://doi.org/10.3389/fmicb.2023.1164877.

Toledo, R., Tomas-Navarro, M., Yuste, J.E., et al., 2024. An update on citrus polymethoxyflavones : chemistry , metabolic fate , and relevant bioactivities. Eur. Food Res. Technol. 250 (8), 2179–2192. https://doi.org/10.1007/s00217-024-04529-5.

Wang, L., Guo, G., Xu, Y., et al., 2024a. The effect of fecal microbiota transplantation on antibiotic-associated diarrhea and its impact on gut microbiota. BMC Microbiol. 24 (1), 160. https://doi.org/10.1186/s12866-024-03261-0.

Wang, N., Dilixiati, Y., Xiao, L., et al., 2024b. Different short-chain fatty acids unequally modulate intestinal homeostasis and reverse obesity-related symptoms in lead-exposed high-fat diet mice. J. Agric. Food Chem. 72 (34), 18971–18985. https://doi.org/10.1021/acs.jafc.4c04193.

Xie, Y., Liu, F., 2024. The role of the gut microbiota in tumor , immunity , and immunotherapy. Front. Immunol. 15, 1410928. https://doi.org/10.3389/fimmu.2024.1410928.

Xu, B., Liang, S., Zhao, J., et al., 2022. Bifidobacterium animalis subsp . lactis XLTG11 improves antibiotic-related diarrhea by alleviating inflammation , enhancing intestinal barrier function and regulating intestinal flora. Food Funct. 13 (11), 6404–6418. https://doi.org/10.1039/d1fo04305f.

Yan, J., Zhang, R., Kang, J., et al., 2023. Effect of Cichorium glandulosum on intestinal microbiota and bile acid metabolism in db/db mice. Food Sci. Nutr. 11 (12), 7765–7778. https://doi.org/10.1002/fsn3.3694.

Yang, S., Qiao, J., Zhang, M., et al., 2024. Prevention and treatment of antibiotics-associated adverse effects through the use of probiotics: a review. J. Adv. Res. https://doi.org/10.1016/j.jare.2024.06.006.

Yanlong, C., Leshan, Z., Xin, W., et al., 2022. Roles of intestinal Parabacteroides in human health and diseases. FEMS Microbiol. Lett. 369 (1), c72. https://doi.org/10.1093/femsle/fnac072.

Yoon, S., Lee, G., Yu, J., et al., 2022. Distinct changes in microbiota-mediated intestinal metabolites and immune responses induced by different antibiotics. Antibiotics 11 (12), 1762. https://doi.org/10.3390/antibiotics11121762.

Yu, X.J., Cong, Z.F., Wang, C.L., et al., 2022. Comprehensive metabolism study of tangeretin in rat plasma, urine and faeces using ultra-high performance liquid chromatography-Q exactive hybrid quadrupole-orbitrap high-resolution accurate mass spectrometry, 23 (12), 973–990. https://doi.org/10.2174/1389200224666221124103611.

Yu, W., Huang, G., Wang, J., et al., 2024. Imperata cylindrica polysaccharide ameliorates intestinal dysbiosis and damage in hyperuricemic nephropathy. Int. J. Biol. Macromol. 278, 134432. https://doi.org/10.1016/j.ijbiomac.2024.134432.

Zhan, M., Yang, X., Zhao, C., et al., 2024. Dietary nobiletin regulated cefuroxime - and levofloxacin-associated " gut microbiota-metabolism " imbalance and intestinal barrier dysfunction in mice. Food Funct. 15 (3), 1265–1278. https://doi.org/10.1039/d3fo04378a.

Zhao, R., Fajardo, J., Shen, G.X., 2023. Influence of Brown or germinated Brown rice supplementation on fecal short-chain fatty acids and microbiome in diet-induced insulin-resistant mice. Microorg. 11 (11), 2629. https://doi.org/10.3390/microorganisms11112629.

Zhou, X., Liang, L., Sun, B., et al., 2024a. The effects of yeast protein on gut microbiota in mice when compared with soybean protein and whey protein isolates. Nutrients 16 (3), 458. https://doi.org/10.3390/nu16030458.

Zhou, M., Ma, J., Kang, M., et al., 2024b. Flavonoids , gut microbiota , and host lipid metabolism. Eng. Life Sci. 24 (5), 2300065. https://doi.org/10.1002/elsc.202300065.